Preparation of silver nanoparticles in the presence of chitosan by electrochemical method

Fikry M. Reicha [a], Afaf Sarhan [a], Maysa I. Abdel-Hamid [a], Ibrahim M. El-Sherbiny [b],*

[a] Biological Advanced Materials, Physics Department, Faculty of Science, Mansoura University, ET-35516 Mansoura, Egypt
[b] Polymer Laboratory, Chemistry Department, Faculty of Science, Mansoura University, ET-35516 Mansoura, Egypt

ARTICLE INFO

ABSTRACT

The present study involves the development of stabilized and densely dispersed chitosan-silver nanoparticles using a green approach based on electrochemical oxidation/complexation process followed by UV irradiation reduction. Formation of the nanoparticles was confirmed by appearance of surface plasmon absorption around 420 nm. The nanoparticles were characterized using transmission electron microscopy, X-ray diffraction, elemental analysis, atomic absorption, energy dispersive X-ray, Fourier transform infrared, and UV–Visible spectrophotometry. The obtained nanoparticles were uniform and spherical with average size of 2–16 nm. It was found that increasing the Ag content in the chitosan-Ag based films tends to decrease their equilibrium swelling values. The nanoparticles also demonstrated a relatively high antibacterial activity against *Bacillus thuringiensis* and *Pseudomonas aeruginosa* bacteria as compared to that of chitosan and the antibacterial activity increased with increasing the nanoparticle concentration. The obtained results revealed that the prepared nanoparticles could be tailored and used in various biomedical applications.

1. Introduction

A significant body of research has focused recently on the development and characterization of nanoparticles (NPs) based on noble metals (Ag, Au, Pt and Pd) because of their remarkable characteristics compared to bulk metals (Evanoff & Chumanov, 2005; Hamanaka, Fukuta, & Nakamura, 2004; He, Kunitake, & Nakao, 2003; Sun et al., 2006; Wang, Qiao, Chen, Wang, & Ding, 2005; Wiley, Sun, Mayers, & Xia, 2005). These noble metals-based NPs were prepared using different approaches including: (a) the chemical reduction of metal precursors with the aid of a reducing agent such as citrate, NaBH$_4$ and ascorbate (Ding, Qian, Tan, & Wang, 2006; Setua et al., 2007; Tan, Qian, Ding, & Wang, 2006), (b) the irradiation of solutions containing metal ions with visible light, ultraviolet (Ghosh, Kunda, & Pal, 2002), or via microwave and ultrasound irradiation (Callegari, Tonti, & Chergui, 2003; Chiu, Chiou, Hsieh, Chen, & Chang, 2005; Mallikarjuna & Varma, 2007; Rocha, Winnischofer, Westphal, & Zanchet, 2007), and (c) the use of bioorganisms and biomolecules, such as bacteria, polysaccharides, and proteins (Chandran, Chaudhary, Pasricha, Ahmad, & Sastry, 2006; D'Souza & Bhainsa, 2006; Lengke, Fleet, & Southam, 2007; Shankar et al., 2004; Willner, Baron, & Willner, 2006).

Silver NPs (Ag NPs) have attracted much interest due to their superior antibacterial characteristics as compared to bulk Ag because of their high surface area, leading to including more NPs within the bacteria and consequently promoting its efficiency in a sustained way (Bajpai, Mohan, Bajpai, Tankhiwale, & Thomas, 2007; Cho, Park, Osaka, & Park, 2005).

Several methods have been reported in the literature for the synthesis of Ag NPs. These methods include; microemulsion (Xie, Ye, & Liu, 2006; Zhang, Qiao, & Chen, 2006), photoreduction (Khanna, Singh, Charan, Subbarao, et al., 2005), chemical reduction (Khanna, Singh, Charan, & Viswanath, 2005; Ryu et al., 2005), γ-radiation (Chen, Song, & Liu, 2007), laser ablation (Tsuji, Watanabe, & Tsuji, 2003), supercritical liquid (Chang, Chang, Lo, Tzing, & Ling, 2003), and magnetron sputtering (Xiong et al., 2000). Many of these techniques showed good control over the particle size and morphology, and the obtained Ag NPs demonstrated superior characteristics. However, most of these methods rely particularly on the use of non safe organic solvents such as dimethyl formamide (DMF), and toxic reducing agents such as sodium borohydride. In addition, these used chemicals are reactive and represent potential biological and environmental risks (Vigneshwaran, Nachane, Balasubramanya, & Varadarajan, 2006). Even the physical methods utilized for the preparation of Ag NPs require relatively sophisticated equipments and specific conditions.

Electrochemical technique was used for the first time to synthesize NPs by Reetz and Helbig (1994). In their setup, a metal sheet was anodically dissolved and the resulting intermediate metal ions

were reduced at the cathode, forming metallic particles stabilized by tetraalkylammonium salts. This was then adopted for the synthesis of the Ag NPs in acetonitrile containing tetrabutylammonium salts (Rodrıguez-Sanchez, Blanco, & López-Quintela, 2000). Using a similar strategy, Ag NPs were prepared by potentiostatic or galvanostatic polarisation of Ag in alcoholic solution (Starowicz, Stypuła, & Banas, 2006). Also, poly(N-vinyl pyrrolidone) (PVP) has been used as a stabilizer during the electrochemical synthesis of Ag particles (Yin, Ma, Wang, & Chen, 2003). However, to the best of our knowledge, there have been no reported studies to date on the preparation of chitosan-Ag NPs through the electrochemical oxidation/complexation process followed by UV irradiation reduction. The present study was devoted to investigate the green synthesis of long-lived chitosan-Ag NPs via the electrochemical oxidation of Ag metal into Ag^+ with in situ complexation with the chitosan followed by UV irradiation reduction of the resulting water soluble chitosan-Ag complex into stabilized and densely dispersed chitosan-Ag NPs.

Chitosan, a cationic polymer obtained through the alkaline N-deacetylation of natural chitin, has been selected in the current study to develop the Ag NPs due to its various superior properties such as non toxicity, biodegradability, biocompatibility (Muzzarelli, 2009), and its high ability to chelate metal ions including Ag^+ (Muzzarelli, 2011). Also, chitosan exhibits good antibacterial activity (Hong, Park, Lee, & Meyers, 2002; Muzzarelli et al., 1990), which would further enhance the antibacterial characteristics of the Ag NPs. Moreover, chitosan has been utilized as stabilizer for the Ag NPs obtained through both the chemical and photochemical reduction methods (Huang et al., 2010).

2. Experimental

2.1. Materials

Commercially chitosan powder, from crab shells, with a degree of deacetylation more than 85% and silver plate (20 mm × 40 mm × 5 mm) of purity 99.99%, were purchased from Sigma–Aldrich (St. Louis, USA). The silver plate was well polished before use with the aid of a very fine emery paper, cleaned by acetone, ethanol (90%) and de-ionized water, and used as working electrode (anode). Platinum rectangular sheet (20 mm × 40 mm × 2 mm) obtained from Sigma, was well cleaned before use as counter electrode (cathode). Acetic acid of analytical grade was provided by the Fine Chemical EL-Nasr Co. (Cairo, Egypt). All other reagents were of analytical grade and used as received. De-ionized water (resistivity > $2 × 10^8$ Ω cm) was used for all samples preparation.

2.2. Methods

2.2.1. Preparation of chitosan-Ag NPs

The chitosan-Ag NPs were prepared through the electrochemical oxidation/complexation followed by UV-irradiation reduction method. The electrochemical oxidation process was carried out using a potentiostatic method in a one compartment electrochemical cell at a constant potential of 2 V. The used cell consists of 5 cm-separated silver (anode) and platinum (cathode) plates. The two electrodes were immersed vertically in the electrolytic solution through platinum wires which sealed to a glass tube. The electrical contact was made via a small mercury pool on the enclosed end of the electrodes and connected to a suitable variable resistor, Picometer (Keithly 485), voltmeter (Keithly 175) and potential power supply (ECOS). The electrolytic solution was prepared by dissolving 1 wt% of chitosan into acetic acid solution (1%) with stirring overnight until complete dissolution and to remove any

bubbles. Nitrogen gas was flushed into the electrolyte during all the preparation process. The temperature was held constant at 25 °C with the aid of a circular water bath (VEB MLW, Type U4; GDR). A thermocouple with an accuracy ±0.1 °C was immersed into the solution to measure its temperature. The electrolytic cell and all other detachable parts of the apparatus were cleaned, before use, with chromic acid mixture and thoroughly washed several times with distilled water and finally with de-ionized water. The strips were first polished with a fine grade emery paper (G400) in order to obtain a smooth surface then immersed in nitric acid and rinsed with de-ionized water. The electrochemical process was carried out for different intervals (6, 12, 18, and 24 h). At the end of electrochemical process, the solution was centrifuged at speed (5000 rpm for 5 min) and filtered to remove any debris (metal particles in the solution). Afterward, a reduction process was performed for the resulting chitosan-Ag complexes into NPs via UV irradiation with the aid of a UV-lamp at $\lambda_{max} = 254$ nm at 25 °C with a constant stirring for different irradiation times (1, 3, and 6 h).

2.3. Instrumental analyses

Elemental analysis of the developed chitosan-Ag complexes and NPs was performed using PerkinElmer 2400 Elemental Analyzer. Atomic absorption spectrometry was also recorded for the prepared samples by Varian spectrometer (spectra AA220) at a λ of 328.1 nm (detection limit (dl) of 0.02 µg/ml) to measure the Ag content in the obtained chitosan-Ag NPs. The UV–Visible spectra of the chitosan-Ag complexes and NPs were recorded in the range of 200–800 nm using ATI Unicom UV–Vis spectrophotometer with the aid of ATI Unicom UV–Vis vision software V 3.20. The analysis was performed at room temperature using quartz cuvettes (1 cm optical path), and the blank was the corresponding chitosan aqueous solution. FTIR spectra were recorded at 25 °C using a Mattson 5000 FTIR spectrometer in the range of 400–4000 cm^{-1} at a resolution of 8 cm^{-1}. A drop of diluted chitosan-Ag samples was spread onto planar freshly cleavage sodium chloride disks. The solvent was completely pumped out at a temperature of 50 °C. Then, the disks were placed in the sample holder of the spectrometer. The morphology of the resulting chitosan-Ag NPs was investigated by TEM (JEOL TEM-1230) attached to a CCD camera at an accelerating voltage of 120 kV. The samples were prepared by placing few drops of the NPs suspension on carbon coated copper grids, followed by allowing the solvent to slowly evaporate overnight at room temperature and under vacuum before recording the TEM images. The microstructure of the chitosan-Ag NPs was also examined using a scanning electron microscope (Philips XL 30 SEM) attached with an energy-dispersive X-ray (EDX) unit, operated at accelerating voltage of 25 kV. The X-ray diffraction patterns of the selected chitosan-Ag samples were obtained using Philips PW 1390 X-ray diffractometer. The X-ray diffraction was provided with a beam monochromator and Cu Kα radiation at $\lambda = 1.5406$ Å. The applied voltage was 40 kV and the current intensity was 40 mA s. The 2θ angle was recorded in the range of 40–60°, and the X-ray runs were carried out at scanning speed of 2°/min. The crystallinity of the developed samples was also calculated with the aid of Material Studio Vision (MSV) software, version 4.4.

2.4. Swelling studies

The chitosan-Ag samples resulting from the electrochemical process were casted in 15 cm Petri dishes and air-dried at room temperature followed by drying at 50 °C for 2 days. Film samples (3 cm × 4 cm) were then cut from the pure chitosan and chitosan-Ag films. The thickness of the films was found to be in the range of 250–300 µm as measured by a digital micrometer. The swelling

behavior was tested by immersing the weighed film samples in de-ionized water at room temperature for predetermined intervals. The sample weights were then determined as function of time after blotting the film with a tissue paper to remove surface water. The swelling percentage (*S%*) of the samples was determined using the following relationship:

$$S\% = \left[\frac{W_s - W_d}{W_d}\right] \times 100$$

where W_d is the weight of the dry sample and W_s is the weight of the swelled sample at time *t*.

2.5. Assessment of the antibacterial activity

The antibacterial activity of chitosan and the chitosan-Ag NPs developed at different times (6, 12, 18, and 24 h) before and after 6 h of UV irradiation reduction was evaluated against *Pseudomonas aeruginosa* and *Bacillus thuringiensis* using the nutrient agar disc diffusion method with determination of the inhibition zones (mm). Briefly, sterile paper discs (6 mm) were impregnated overnight in sample solutions and then left to dry at 37 °C for 24 h in sterile conditions. The bacterial suspensions were obtained by making a saline suspension of isolated colonies selected from 18 to 24 h of nutrient agar plating. The suspensions were adjusted to match the tube of 0.5 McFarland turbidity standards with the aid of spectrophotometry at 600 nm, which equals 1.5×10^8 colony-forming units/ml. The surface of the nutrient agar was completely inoculated using a sterile swab, which was steeped in the prepared bacterial suspension. Then, the impregnated discs were placed on the inoculated agar and incubated for 24 h at 37 °C. After incubation, the diameters of the growth inhibition zones were measured.

3. Results and discussion

3.1. Preparation of the chitosan-Ag NPs

Densely dispersed and stabilized (for more than 6 months) chitosan-Ag NPs have been prepared in the current study with the aid of a new green preparation method. This method depends particularly on the electrochemical oxidation of Ag anode into Ag$^+$ with in situ complexation with the chitosan dissolved in an acidic

electrolyte solution followed by a UV irradiation reduction of the resulting water soluble complex into chitosan-Ag NPs. The chitosan ability to chelate the resulting Ag$^+$ ions originates particularly from the presence of NH$_2$ and OH groups in the β(1–4) D-glucosamine units of the chitosan.

The electrochemical complexation process was carried out for different times (6, 12, 18, and 24 h). The formation of the water soluble chitosan-Ag complex was confirmed with the aid of UV–Vis spectra of the samples through appearance of absorption peaks at about 250 nm, as apparent in Fig. 1a which is in agreement with the literature (Rahz et al., 2002). With time, an equilibrium was attained and a saturation of the electrolyte solution with the chitosan-Ag complex occurred. This led to an electrochemical reduction of some of the water soluble complex at the cathode forming chitosan-Ag NPs with turning the colorless electrolyte solution into pale yellow. This color became darker until brown with increasing the process time. The formation of chitosan-Ag NPs through electrochemical reduction was also confirmed using UV–Vis spectrophotometry through the appearance of absorption peaks at around 420 nm, starting from a process time of 12 h, as shown in Fig. 1a. The intensities of the absorption increased with increasing the electrochemical process time up to 24 h. These peaks around 420 nm are corresponding to the characteristic surface plasmon resonance of the formed chitosan-Ag NPs (Wang, Zhuang, Peng, & Li, 2005). Increasing the peak intensity indicated that the concentration of the obtained chitosan-Ag NPs increases with time (Zhang et al., 2006).

It has been found that the maximum time for the electrochemical complexation process is 24 h. Beyond this time, the Ag$^+$ released from the anode oxidation undergoes reduction into metallic Ag due to the consumption of the chitosan molecules able to chelate with the Ag$^+$ ions. This has been confirmed via appearance of Ag powder in the bottom of the electrochemical cell and also through the X-ray analysis of the precipitated powder.

The water soluble chitosan-Ag complexes remaining from the electrochemical stage were then reduced via UV irradiation for different time intervals (1, 3, and 6 h) into densely dispersed chitosan-Ag NPs. The formation of the chitosan-Ag NPs after 1 h of UV irradiation can be noted from Fig. 1b. This figure shows the absorption peaks at about 420 nm corresponding to the characteristic surface plasmon resonance of the resulting chitosan-Ag NPs
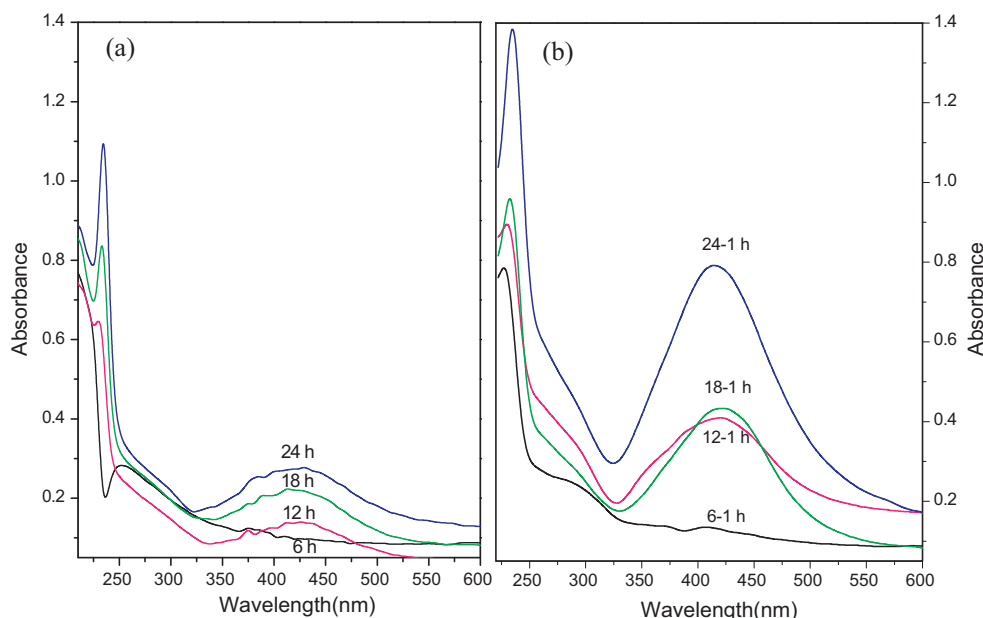

Fig. 1. UV–Vis spectra of the ionic chitosan-Ag complexes and the obtained chitosan-Ag NPs: (a) before, and (b) after UV-irradiation reduction.
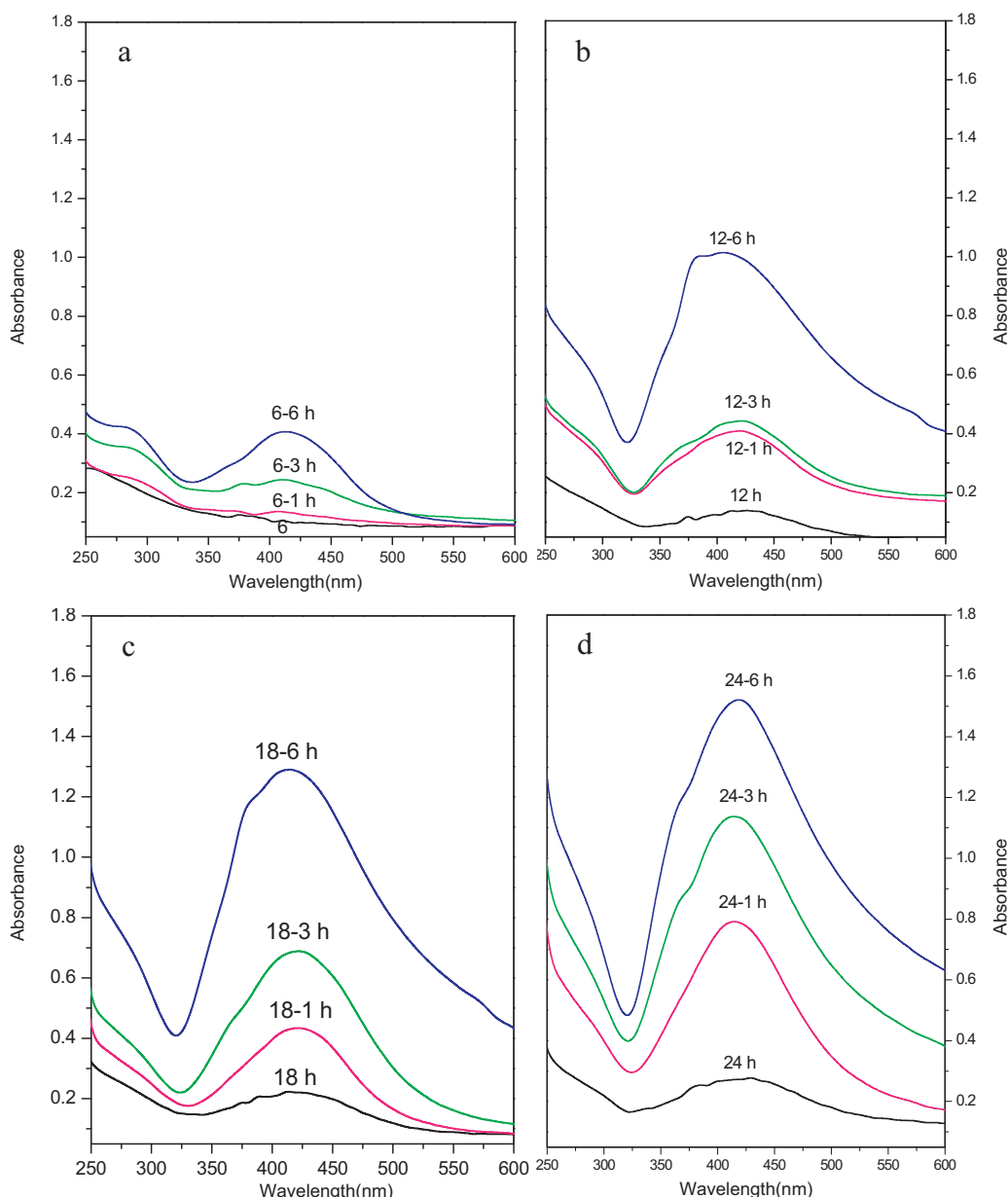
Fig. 2. UV–Vis spectra of the chitosan-Ag NPs resulting from electrochemical complexation of chitosan and Ag⁺ ions for different times (6, 12, 18, and 24 h) followed by UV irradiation reduction for different time periods (0, 1, 3, and 6 h).

(Wang, Qiao, et al., 2005). Comparing the peak intensities of the samples after UV irradiation (Fig. 1b) with the same samples before UV irradiation (Fig. 1a) demonstrates a considerable increase in the peak intensities which reflects a significant increase in the concentration of the resulting chitosan-Ag NPs upon irradiation. During the electrochemical oxidation step, the resulting ionic chitosan-Ag complexes are expected to be reduced by the hydrated electrons (e_{aq}^-) which formed upon irradiation of the solution (Bogle, Dhole, & Bhoraskar, 2006; Zhu, Qian, Li, & Zhang, 1997). Then, the Ag atoms in the chitosan-Ag, produced from the irradiation reduction step were aggregated through metallic bonding to form the Ag core of the NPs. The molecular orbitals in the formed Ag clusters accommodate electrons, which are delocalized and occupy the lowest energy orbitals to stabilize the Ag core (Medina-Ramirez, Bashir, Luo, & Liu, 2009). Presence of chitosan is important for the stabilization of the formed NPs as it prevents the Ag clusters from aggregation at the macroscopic level due to the ion–dipole intermolecular forces (Shameli et al., 2010).

The formation of the chitosan-Ag NPs was also confirmed from comparing the UV–Vis spectra of the chitosan-Ag samples subjected to different times of UV irradiation reduction as shown in Fig. 2. From the figure, it is obvious that, with keeping the time of the electrochemical process constant, increasing the time of UV irradiation reduction led to a significant increase in the intensity of the absorption peak corresponding to the surface plasmon resonance and consequently in the concentration of the formed chitosan-Ag NPs. Also, from the figure, it can be noted that the maximum absorption wavelength (λ_{max}) was blue shifted with increasing the time of UV irradiation. This blue shift implies a decrease in the size of the resulting chitosan-Ag NPs with irradiation time (Shameli et al., 2010).

The formation of chitosan-Ag NPs was also confirmed from the appearance of strong Ag signals in the EDX spectra of the chitosan-Ag samples recorded after 24 h of electrochemical process followed by 1 h of UV irradiation reduction (Fig. 3a). Atomic absorption measurements were also used as another evidence as illustrated
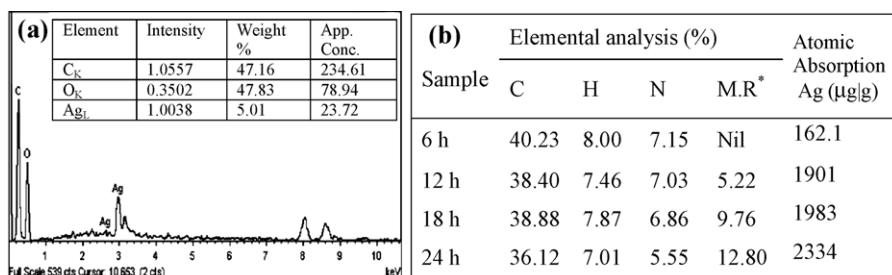
(a) Element	Intensity	Weight %	App. Conc.
C_K	1.0557	47.16	234.61
O_K	0.3502	47.83	78.94
Ag_L	1.0038	5.01	23.72

(b) Sample	Elemental analysis (%)				Atomic Absorption Ag ($\mu g|g$)
	C	H	N	M.R[*]	
6 h	40.23	8.00	7.15	Nil	162.1
12 h	38.40	7.46	7.03	5.22	1901
18 h	38.88	7.87	6.86	9.76	1983
24 h	36.12	7.01	5.55	12.80	2334

Fig. 3. (a) The EDX spectra of the chitosan-Ag NPs obtained after 24 h of electrochemical process followed by 1 h of UV irradiation reduction and (b) elemental analysis, and atomic absorption of the developed chitosan-Ag complexes and NPs (*M.R.: metallic residue %).

in Fig. 3b. From the figure, increasing the process time led to a statistically significant increase in the Ag content ($\mu g/g$). For instance, increasing the time of electrochemical process from 6 h to 24 h has increased the Ag content from 162.1 to 2334 $\mu g/g$. The incidence of complexation and NPs formation can also be deduced from the decreasing of N-content, representing the chitosan molecules, upon comparing the measured elemental analysis data of the samples obtained at different process times (Fig. 3b).

3.2. FTIR spectroscopy

Fig. 4 shows the FTIR spectra of the chitosan-Ag samples resulting after 24 h of electrochemical process before and after 1 h of UV irradiation reduction, in comparison with that of the chitosan. In the case of chitosan, the spectra demonstrated a peak at about 3300–3430 cm^{-1} which can be assigned for the O—H stretching vibration and the N—H extension vibration of the polysaccharide moieties of chitosan. The signal appeared around 2890 cm^{-1} is corresponding to the stretching vibrations of the aliphatic C—H bonds

whereas, the peak noted at 1637 cm^{-1} is due to the stretching vibration of the amide "C=O" bond. The spectra of the chitosan-Ag sample, obtained at 24 h of electrochemical process exhibited a few alterations from that of chitosan. For instance, the peak appeared in the chitosan spectrum at 3300–3430 cm^{-1} has showed a relative decrease of transmittance indicating that the N—H vibration was affected due to the attachment of the NH$_2$ groups of chitosan with the Ag$^+$ ions during the electrochemical process (Jin & Bai, 2002). Also, a relative reduction in the intensity of the peak at 1637 cm^{-1} has been noted due to the deformation vibration of the amine groups of chitosan. All the other peaks of chitosan almost maintained their position in the corresponding chitosan-Ag sample, but with a change in their peak intensity. The FTIR spectra of the chitosan-Ag sample subjected to UV irradiation reduction did not show a significant change from the corresponding spectra before UV irradiation and it tends to further confirm the interaction between the NH$_2$ and OH groups of the chitosan with the Ag.

3.3. Transmission electron microscopy (TEM)

The typical transmission electron microscopy (TEM) images and the corresponding particle size distribution of the chitosan-Ag NPs developed at different times (12 and 18 h) of electrochemical complexation followed by 1 h of UV irradiation reduction are shown in Fig. 5. As Fig. 5 demonstrates, the obtained chitosan-Ag NPs are in the nano range with uniform, and spherical shapes. The chitosan-Ag NPs obtained after 12 h of electrochemical process followed by 1 h of UV irradiation (Fig. 5a and b) showed average diameters from 10 to 16 nm. This particle size range was decreased to 2–8 nm in the case of the chitosan-Ag NPs resulting after 18 h of electrochemical process followed by 1 h of UV irradiation (Fig. 5c and d). This is in agreement with the blue shift observed in the UV–Vis spectra of these samples and discussed in Section 3.1. The figure also revealed that the chitosan-Ag NPs are well dispersed which indicates a good stabilization effect of the chitosan. Fig. 5e represents the diffraction pattern of some developed chitosan-Ag NPs. Although, the diffraction patterns seem to be a little diffused due to the small particle size, three diffraction bands were clearly noted. These diffractions can be indexed to the face-centered cubic structure of the Ag lattice. The closest diffraction band to the center and almost the strongest one is probably a combination of the (1 1 1) and (2 0 0) reflections. The second band is likely representing the (2 2 2) reflection, whereas the outermost and the weakest third band is either the (4 2 0) or the (4 2 2) reflection.

3.4. X-ray diffraction analysis

Fig. 6a shows the X-ray diffraction patterns of chitosan-Ag samples resulting at different times of electrochemical process as compared to chitosan. The X-ray diffraction pattern of pure chitosan showed three weak bands at 2θ values of 10.1°, 15.4° and 20.4°, indicating an almost amorphous nature of the chitosan used
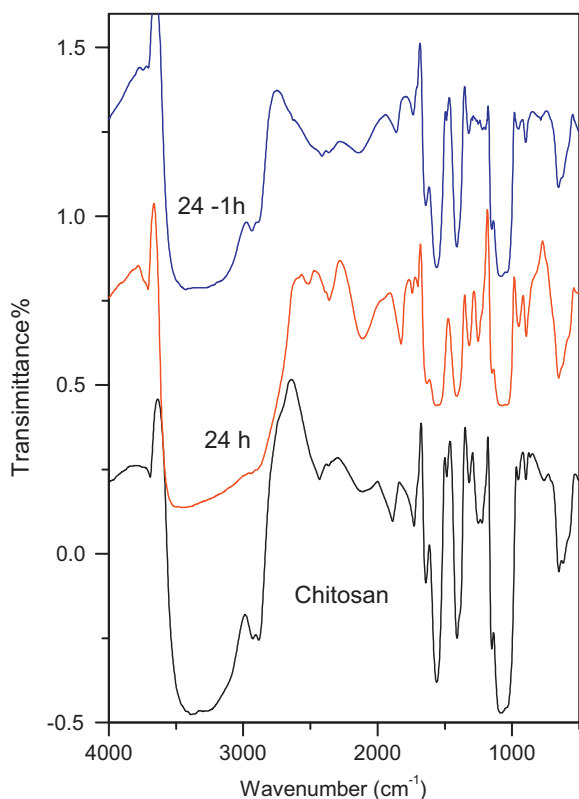

Fig. 4. FTIR spectra of chitosan and the chitosan-Ag NPs resulting after 24 h of electrochemical process and after 24 h of electrochemical process followed by 1 h of UV irradiation reduction.
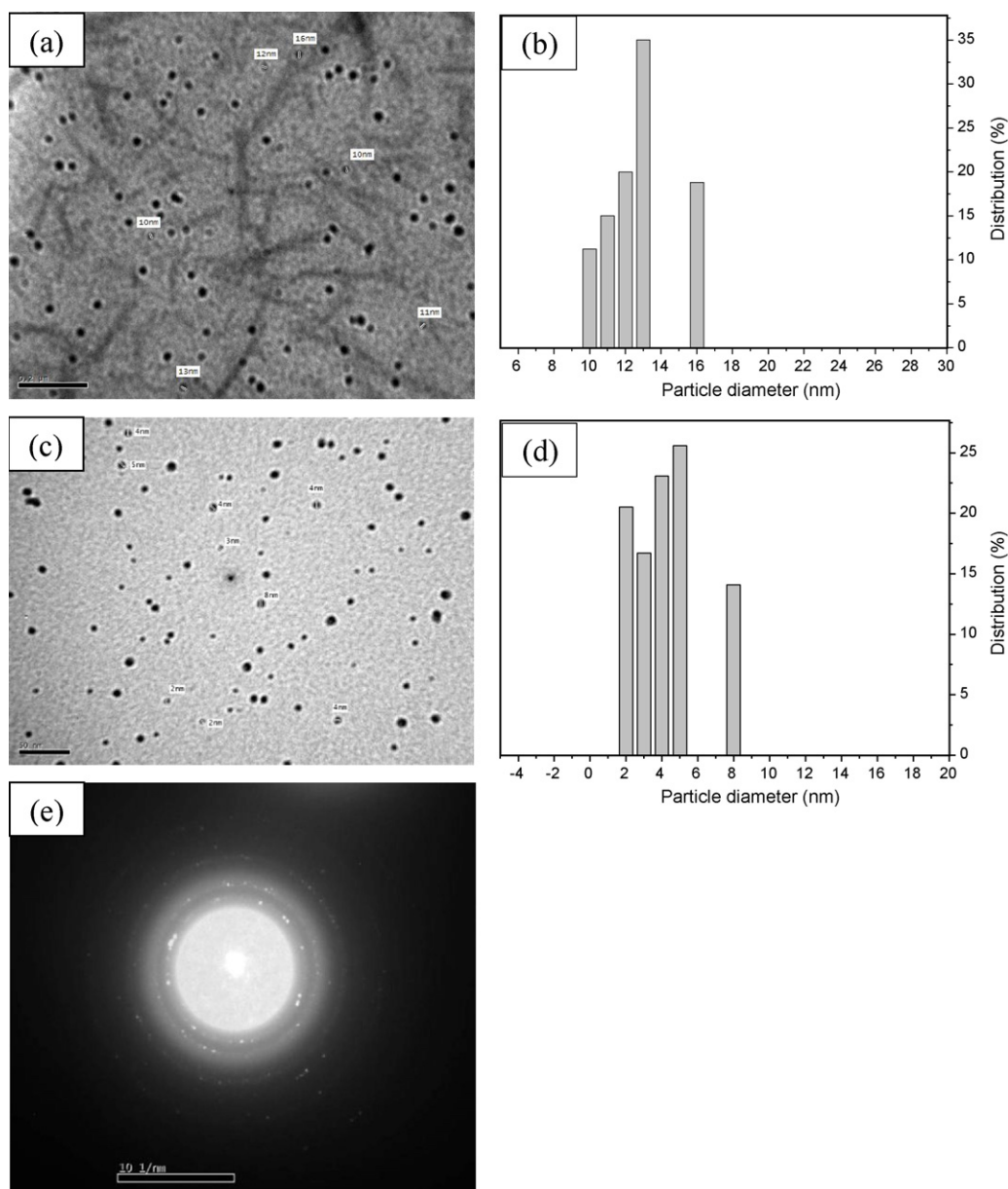
Fig. 5. The typical TEM images and the corresponding particle size distribution, and the diffraction pattern of the developed chitosan-Ag NPs at different electrochemical process times; (a and b) 12 h, and (c–e) 18 h, followed by 1 h of UV irradiation reduction.

in the current study which is in agreement with the literature (Seo, Koh, Roh, & Kim, 2009). In the diffractograms of the chitosan-Ag samples, the two peaks at the 2θ values of 10.1° and 15.4° of the pure chitosan almost disappeared and the one at 2θ of 20.4° became broader which reflects a more amorphous nature (Seo et al., 2009).

Fig. 6b demonstrates the X-ray diffraction patterns of chitosan-Ag samples produced after 24 h of electrochemical process before and after heat treatment at 120 °C. The heat treated samples showed the existence of some crystalline peaks appearing at 2θ values of 38° and 44° which can be attributed to the reflection planes (1 1 1) and (2 0 0) of the Ag clusters within the chitosan-Ag matrices. These results are in agreement with standard values and confirm the Ag reduction and growth (Hu, Kong Ch Han, Zhao, Yang, & Wu, 2007).

The X-ray diffraction analysis was also performed to investigate the crystallinity pattern of the chitosan-Ag NPs obtained after UV irradiation reduction as shown in Fig. 6c. From the figure, the small peaks appeared at the 2θ values of 9.1°, 38° (1 1 1), and 44.3° (2 0 0)

in the irradiated chitosan-Ag samples may be attributed to the formation of Ag NPs as these diffraction peaks were not observed in the pure chitosan. The intensity of these peaks increased with increasing the irradiation time. Increasing the degree of crystallinity of the chitosan-Ag NPs with increasing the time of electrochemical process followed by 6 h of UV irradiation reduction was also confirmed with the aid of Material Studio Vision software as depicted in Fig. 6d (Seo et al., 2009).

3.5. Swelling studies

Swelling ability of polymer films and nanocomposites is one of the main characteristics that determines their suitability for many biomedical applications. The swelling behavior of various films based on chitosan-Ag NPs obtained at different times of electrochemical process (12, 18, and 24 h) and different times of UV irradiation reduction (1, 3, and 6 h) are shown in Fig. 7.
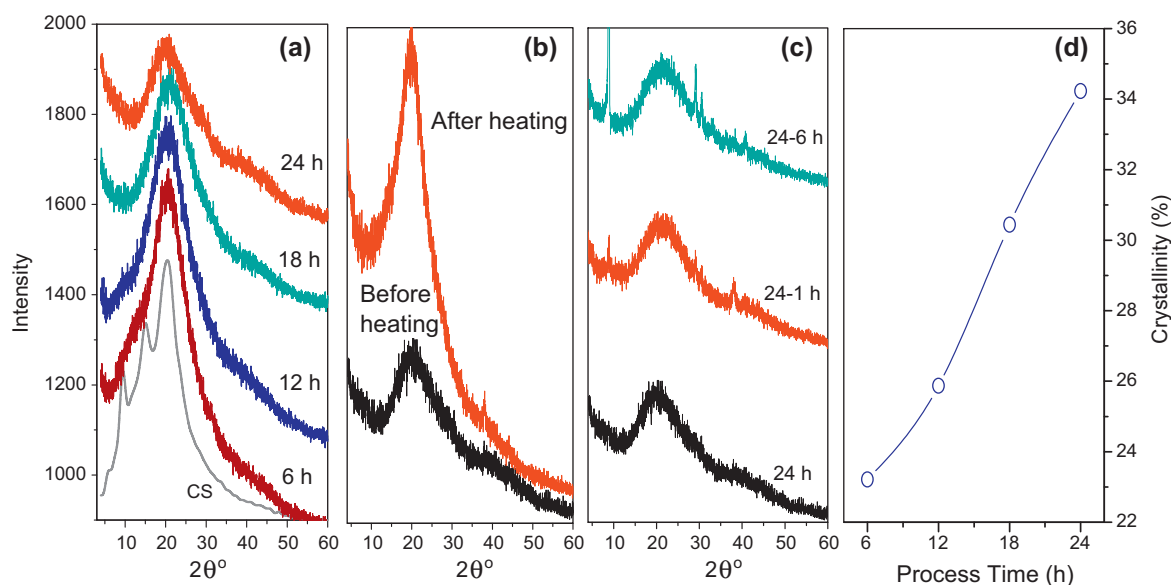
Fig. 6. XRD patterns of (a) chitosan-Ag samples resulting at different times of electrochemical process as compared to chitosan alone, (b) chitosan-Ag NPs produced after 24 h of electrochemical process before and after heat treatment at 120 °C, (c) chitosan-Ag NPs resulting at 24 h of electrochemical oxidation followed by UV irradiation reduction for different times (1 and 6 h), and (d) degree of crystallinity (%) estimated with the aid of Material Studio Vision (MSV 4.4) software for the chitosan-Ag NPs resulting at different times of electrochemical process (6, 12, 18, and 24 h), followed by 6 h of UV irradiation reduction.

From Fig. 7a, it can be noted that increasing the Ag content in the chitosan-Ag based films upon increasing the time of the electrochemical process from 12 h to 24 h tends to decrease the swelling values attained at equilibrium. Also, the maximum swelling values decreased significantly with increasing the Ag content upon increasing the UV irradiation time from 1 to 6 h as apparent in Fig. 7b. This reduction in swelling values may be attributed to the acting of the Ag as crosslinkers between chitosan chains. These crosslinking points increase with increasing the Ag content in the matrices which reduces the mobility of the chitosan chains and consequently reduces the swelling extent of the films.

3.6. Antibacterial studies

The inhibition zone values were determined for the prepared chitosan-Ag NPs tested against two types of bacteria, *B. thuringiensis* and *P. aeruginosa*. Results and images for the inhibition zones were presented as average values (mm) as shown in Fig. 8. The obtained data demonstrates that all the investigated chitosan-Ag NPs had relatively high and almost similar antibacterial activity against Gram-positive (*B. thuringiensis*) and Gram-negative (*P. aeruginosa*) bacteria as compared to that of control (chitosan). This relatively high antibacterial activity can be attributed to the size and the high surface area of the chitosan-Ag NPs which enabled them to reach
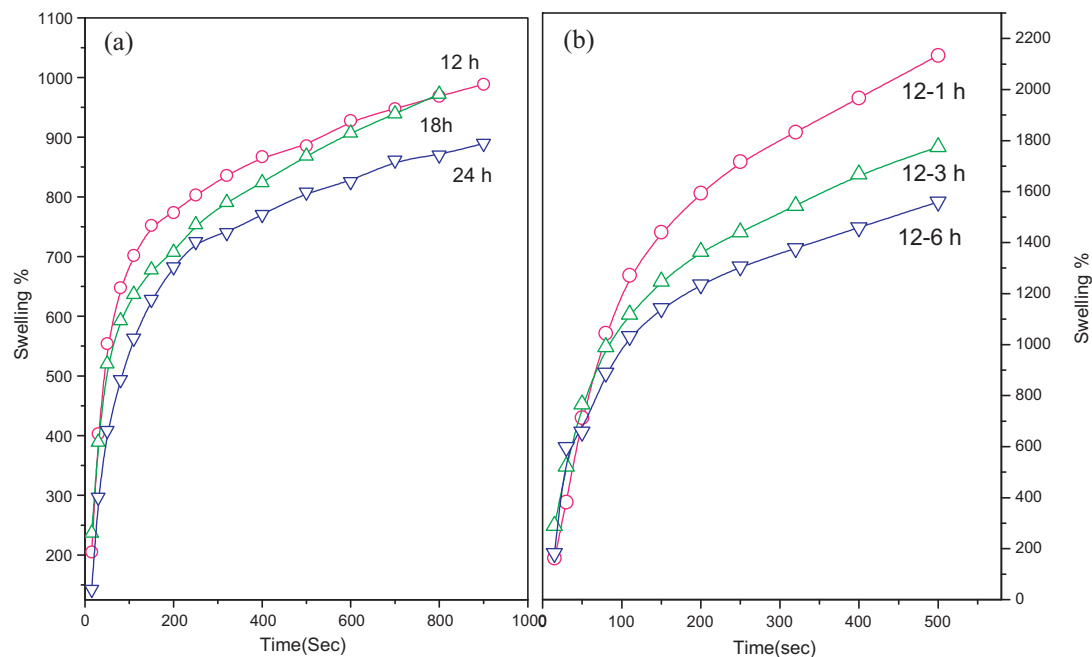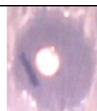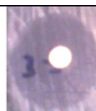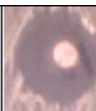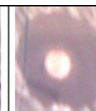

Fig. 7. Swelling patterns of films prepared by casting of the chitosan-Ag samples resulting at (a) different times of electrochemical process (12, 18, and 24 h), and (b) 12 h of electrochemical process followed by different times of UV irradiation reduction (1, 3, and 6 h).

B. thuringiensis (Gram-positive)	Chitosan	6 h	12 h	18 h	24 h	6-6 h	12-6 h	18-6 h	24-6 h
Inhibition zones (mm)	24	27	28	30	35	36	42	46	47
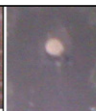
P. aeruginosa (Gram-negative)	Chitosan	6 h	12 h	18 h	24 h	6-6 h	12-6 h	18-6 h	24-6 h
Inhibition zones (mm)	26	30	32	34	35	37	39	42	55

Fig. 8. Comparison between the bacterial inhibition zones (mm) of chitosan and the chitosan-Ag NPs developed at different times (6, 12, 18, and 24 h) before and after 6 h of UV irradiation reduction.

easily the nuclear content of bacteria (Lok, Ho, & Chen, 2006). It is apparent also from the data in Fig. 8 that increasing the concentration of the chitosan-Ag NPs with process time and also upon UV irradiation reduction of the samples for 6 h led to a significant increase in the antibacterial activity. In spite of the strong antibacterial activity of the developed chitosan-Ag NPs, further studies are required to investigate their bactericidal effects on different types of bacteria for potential widening of their applications.

4. Conclusions

In the present study, uniform and densely dispersed chitosan-Ag NPs were prepared using a new green technique. This technique is based on electrochemical oxidation/complexation process followed by UV irradiation reduction. The major advantages of this applied technique include the high purity of the obtained NPs and the possibility of the particle size control via adjusting the current density without a need for vacuum or sophisticated equipments. Moreover, this preparation method is cost-effective, relatively quick and it also offers various advantages of biocompatibility and eco-friendliness for various biomedical and pharmaceutical applications as all the materials used in the study were renewable and environmentally benign.

References

Bajpai, S. K., Mohan, Y. M., Bajpai, M., Tankhiwale, R., & Thomas, V. (2007). Synthesis of polymer stabilized silver and gold nanostructures. *Journal of Nanoscience & Nanotechnology, 7*, 2994–3010.

Bogle, K. A., Dhole, S. D., & Bhoraskar, V. N. (2006). Silver nanoparticle: Synthesis and size control by electron irradiation. *Nanotechnology, 17*, 3204–3208.

Callegari, A., Tonti, D., & Chergui, M. (2003). Photochemically grown silver nanoparticles with wavelength-controlled size and shape. *Nano Letters, 3*, 1565–1568.

Chandran, S. P., Chaudhary, M., Pasricha, R., Ahmad, A., & Sastry, M. (2006). Synthesis of gold nanotriangles and silver nanoparticles using Aloevera plant extract. *Biotechnology Progress, 22*, 577–583.

Chang, J. Y., Chang, J. J., Lo, B., Tzing, S. H., & Ling, Y. C. (2003). Silver nanoparticles spontaneous organize into nanowires and nanobanners in supercritical water. *Chemistry & Physics Letters, 379*, 261–267.

Chen, P., Song, L. Y., & Liu, Y. K. (2007). Synthesis of silver nanoparticles by γ-ray irradiation in acetic water solution containing chitosan. *Radiation Physics and Chemistry, 76*, 1165–1168.

Chiu, T. C., Chiou, S. H., Hsieh, M. M., Chen, Y. T., & Chang, H. T. (2005). Photosynthesis of gold nanoparticles in presence of proteins. *Journal of Nanoscience & Nanotechnology, 5*, 2128–2132.

Cho, K. H., Park, J. E., Osaka, T., & Park, S. G. (2005). The study of antimicrobial activity and preservative effects of nanosilver ingredient. *Electrochimica Acta, 51*, 956–960.

Ding, S. H., Qian, W. P., Tan, Y., & Wang, Y. (2006). Gold-nanoparticle-infiltrated polystyrene inverse opals: A three-dimensional platform for generating combined optical properties. *Langmuir, 22*, 7105–7108.

D'Souza, S. F., & Bhainsa, K. C. (2006). Extracellular biosynthesis of silver nanoparticles using the fungus *Aspergillus fumigatus*. *Colloids and Surfaces B-Biointerfaces, 47*, 160–164.

Evanoff, D. D., & Chumanov, G. (2005). Synthesis and optical properties of silver nanoparticles and arrays. *Chemical Physics, 6*, 1221–1231.

Ghosh, S. K., Kunda, S., & Pal, T. (2002). Bull evolution, dissolution and reversible generation of gold and silver nanoclusters in micelle by UV-activation. *Materials Science, 25*, 581–582.

Hamanaka, Y., Fukuta, K., & Nakamura, A. (2004). Enhancement of third-order non-linear optical susceptibilities in silica-capped Au nanoparticle films with very high concentrations. *Applied Physics Letters, 84*, 4938–4940.

He, J. H., Kunitake, T., & Nakao, A. (2003). Facile in situ synthesis of noble metal nanoparticles in porous cellulose fibers. *Chemistry of Materials, 15*, 4401–4403.

Hong, K. N., Park, N. Y., Lee, S. H., & Meyers, S. P. (2002). Antibacterial activity of chitosans and chitosan oligomers with different molecular weights. *International Journal of Food Microbiology, 74*, 65–72.

Hu, Z., Kong Ch Han, Y., Zhao, H., Yang, Y., & Wu, H. (2007). Large-scale synthesis of defect-free silver nanowires by electrodeless deposition. *Materials Letters, 61*, 3931–3934.

Huang, N. M., Lim, H. N., Radiman, S., Khiew, P. S., Chiu, W. S., Hashim, R., et al. (2010). Sucrose ester micellar-mediated synthesis of Ag nanoparticles and the antibacterial properties. *Colloids and Surfaces A-Physicochemical and Engineering Aspects, 353*, 69–76.

Jin, L., & Bai, R. (2002). Mechanisms of lead adsorption on chitosan/PVA hydrogel beads. *Langmuir, 18*, 9765–9770.

Khanna, P. K., Singh, N., Charan, S., Subbarao, V. V. V. S., Gokhale, R., & Mulik, U. P. (2005). Synthesis and characterization of Ag/PVA nanocomposite by chemical reduction method. *Materials Chemistry and Physics, 93*, 117–121.

Khanna, P. K., Singh, N., Charan, S., & Viswanath, A. K. (2005). Synthesis of Ag/polyaniline nanocomposite via an in situ photo-redox mechanism. *Materials Chemistry and Physics, 92*, 214–219.

Lengke, M. F., Fleet, M. E., & Southam, C. (2007). Biosynthesis of silver nanoparticles by filamentous cyanobacteria from a silver (I) nitrate complex. *Langmuir, 23*, 2694–2699.

Lok, C. N., Ho, C. M., Chen, R., He, Q. Y., Yu, W. Y., Sun, H., et al. (2006). Proteomic analysis of the mode of antibacterial action of silver nanoparticles. *Journal of Proteome Release, 5*, 916–924.

Mallikarjuna, N. N., & Varma, R. S. (2007). Microwave-assisted shape-controlled bulk synthesis of noble nanocrystals and their catalytic properties. *Crystal Growth & Design, 7*, 686–690.

Medina-Ramirez, I., Bashir, S., Luo, Z., & Liu, J. L. (2009). Green synthesis and characterization of polymer-stabilized silver nanoparticles. *Colloids and Surfaces B-Biointerfaces, 73*, 185–191.

Muzzarelli, R. A. A. (2009). Chitins and chitosans for the repair of wounded skin, nerve, cartilage and bone. *Carbohydrate Polymers, 76*, 167–182.

Muzzarelli, R. A. A. (2011). Potential of chitin/chitosan-bearing materials for uranium recovery: An interdisciplinary review. *Carbohydrate Polymers, 84*, 54–63.

Muzzarelli, R. A. A., Tarsi, R., Filippini, O., Giovanetti, E., Biagini, G., & Varaldo, P. E. (1990). Antimicrobial properties of N-carboxybutyl chitosan. *Antimicrobial Agents and Chemotherapy, 34*, 2019–2023.

Rahz, M., Desbrieres, J., Tolaimate, A., Rinaudo, P., Vottero, P., & Alagui, A. (2002). *Polymer, 43*, 1267–1276.

Reetz, M. T., & Helbig, W. J. (1994). Size-selective synthesis of nanostructured transition metal clusters. *Journal of American Chemical Society, 116*, 7401–7406.

Rocha, T. C. R., Winnischofer, H., Westphal, E., & Zanchet, D. (2007). Formation kinetics of silver triangular nanoplates. *Journal of Physical Chemistry C, 111*, 2885–28891.

Rodríguez-Sanchez, L., Blanco, M. C., & López-Quintela, M. A. (2000). Electrochemical synthesis of silver nanoparticles. *Journal of Physical Chemistry B, 104*, 9683–9688.

Ryu, B. H., Choi, Y., Park, H. S., Byun, J. H., Kong, K., Lee, J. O., et al. (2005). Synthesis of highly concentrated silver nanosol and its application to inkjet printing. *Colloids and Surfaces A-Physicochemical and Engineering Aspects, 270–271*, 345–351.

Seo, J. A., Koh, J. H., Roh, D. K., & Kim, J. H. (2009). Preparation and characterization of crosslinked proton conducting membranes based on chitosan and PSSA-MA copolymer. *Solid State Ionics, 180*, 998–1002.

Setua, P., Chakraborty, A., Seth, D., Bhatta, M. U., Satyam, P. V., & Sarkar, N. (2007). Synthesis, optical properties, and surface enhanced Raman scattering of silver nanoparticles in nonaqueous methanol reverse micelles. *Journal of Physical Chemistry C, 111*, 3901–3907.

Shameli, K., Ahmad, M. B., Yunus, W. M. Z. W., Rustaiyan, A., Ibrahim, N. A., Zargar, M., et al. (2010). Green synthesis of silver/montmorillonite/chitosan bionanocomposites using the UV irradiation method and evaluation of antibacterial activity. *International Journal of Nanomedicine, 5*, 875–887.

Shankar, S. S., Rai, A., Ankamwar, B., Singh, A., Ahmad, A., & Sastry, M. (2004). Biological synthesis of triangular gold nanoprisms. *Nature Materials, 3*, 482–488.

Starowicz, M., Stypuła, B., & Banas, J. (2006). Electrochemical synthesis of silver nanoparticles. *Electrochemistry Communications, 8*, 227–230.

Sun, J. M., Ma, D., Zhang, H., Liu, X. M., Han, X. W., Bao, X. H., et al. (2006). Toward monodispersed silver nanoparticles with unusual thermal stability. *Chemical Society, 128*, 15756–15764.

Tan, Y., Qian, W. P., Ding, S. H., & Wang, Y. (2006). Gold-nanoparticle-infiltrated polystyrene inverse opals: A three-dimensional platform for generating combined optical properties. *Chemistry of Materials, 18*, 3385–3389.

Tsuji, T., Watanabe, N., & Tsuji, M. (2003). Laser induced morphology change of silver colloids: Formation of nano-size wires. *Applied Surface Science, 211*, 189–193.

Vigneshwaran, N., Nachane, R. P., Balasubramanya, R. H., & Varadarajan, P. V. (2006). A novel one-pot 'green' synthesis of stable silver nanoparticles using soluble starch. *Carbohydrate Research, 341*, 2012–2018.

Wang, H. S., Qiao, X. L., Chen, J. G., Wang, X. J., & Ding, S. Y. (2005). Mechanisms of PVP in the preparation of silver nanoparticles. *Materials Chemistry and Physics, 94*, 449–453.

Wang, X., Zhuang, J., Peng, Q., & Li, Y. D. (2005). Heavy equipment operator training via virtual modeling technologies. *Nature, 437*, 121.

Wiley, B., Sun, Y. G., Mayers, B., & Xia, Y. N. (2005). Shape-controlled synthesis of metal nanostructures: The case of silver. *Chemistry - A European Journal, 11*, 454–463.

Willner, I., Baron, R., & Willner, B. (2006). Growing metal nanoparticles by enzymes. *Advanced Materials, 18*, 1109–1120.

Xie, Y. W., Ye, R. Q., & Liu, H. L. (2006). Synthesis of silver nanoparticles in reverse micelles stabilized by natural biosurfactant. *Colloids and Surfaces A-Physicochemical and Engineering Aspects, 279*, 175–178.

Xiong, Y. Q., Wu, H., Guo, Y., Sun, Y., Yang, D. Q., & Da, D. A. (2000). Preparation and characterization of nanostructured silver thin films deposited by radio frequency magnetron sputtering. *Thin Solid Films, 375*, 300–303.

Yin, B., Ma, H., Wang, S., & Chen, S. (2003). Electrochemical synthesis of silver nanoparticles under protection of poly (N-vinylpyrrolidone). *Journal of Physical Chemistry B, 107*, 8898–8904.

Zhang, W. Z., Qiao, X. L., & Chen, J. G. (2006). Synthesis and characterization of silver nanoparticles in AOT microemulsion system. *Chemical Physics, 300*, 495–500.

Zhu, Y., Qian, Y., Li, X., & Zhang, M. (1997). γ-Radiation synthesis and characterization of polyacrylamide-silver nanocomposites. *Chemical Communications, 10*, 1081–1082.